Linear Viscoelastic Diffusion in the Poly(styrene)–Ethylbenzene System: Comparison between Theory and Experiment

G. F. Billovits† and C. J. Durning*

Department of Chemical Engineering, Materials Science and Mining, Columbia University, New York, New York 10027

Received May 27, 1994; Revised Manuscript Received September 19, 1994®

ABSTRACT: We compare mutual diffusion data in the poly(styrene)–ethylbenzene system with theory. The experiments[1] were differential vapor sorptions carried out at 40 °C on a thin film over a range of compositions spanning the system's glass transition. Under these conditions, viscoelastic relaxation strongly influences mutual diffusion, so that non-Fickian sorption data are seen. The theories considered[2,3] account for the influence of relaxation by including fading memory in the mixture's free energy density. By fitting the data with the theory, we extracted as a function of ethylbenzene weight fraction, w_1, the mutual binary diffusion coefficient, D_{12}, relaxation times, τ_1 and τ_2 ($>\tau_1$), and the ratio of the high-frequency mechanical modulus to the osmotic modulus, k_0. In the glassy state, D_{12} and τ_1 remain nearly constant, while in the liquid state they change rapidly with w_1 (D_{12} increases; τ_1 decreases). The Vrentas–Duda free volume theory,[4,5] modified to account for the influence of the glass transition,[6,7] can account for the trends. The shorter relaxation time, τ_1, agrees with mechanically measured relaxation times in the transition zone.[8,9] The longer time, τ_2, shows rough agreement with the terminal time,[10,11] although the comparison is not definitive. The ratio k_0 is found to be constant, at $\sim$ O(10) over the entire concentration range, whereas the Flory–Huggins theory predicts that it should slowly increase with w_1; the reasons for the discrepancy are not clear.

Introduction

Mutual diffusion governs the mixing or demixing of components in a binary mixture under an osmotic field. In mixtures of Newtonian fluids, Fick's law adequately describes this process in the continuum limit; however, it often fails when one component is polymeric. The failure is clearly because of the polymer's fading memory since it only occurs when a dominant relaxation time in the mixture matches or exceeds the time scale for interdiffusion. A quantitative understanding of this viscoelastic, non-Fickian diffusion is an important practical goal since many engineering applications involve or rely on it. In this paper we make a careful comparison between viscoelastic diffusion data and theory. The data, reported in ref 1 (referred to as part 1 hereafter), were measured by differential vapor sorption for ethylbenzene (EB) in polystyrene (PS) in the concentrated polymer regime. The experiments probe the long-wavelength dynamics of mutual diffusion in concentrated PS–EB mixtures in a linear perturbation limit. The data show unmistakable viscoelastic features which vary systematically with EB content; they supply a reliable benchmark for comparisons with theory.

During the past decade, more than a dozen theoretical papers have been published addressing viscoelastic diffusion.[12–15] The majority of these rely on nonequilibrium thermodynamics,[12] although statistical mechanic,[13] hydrodynamic,[14] and purely mathematical[15] developments have been pursued. While each of these treatments is general enough to handle multiaxial, nonlinear diffusion problems of a simple fluid and a viscoelastic material (either solid or fluid), none has been tested thoroughly against experiment. In this work we apply two of the nonequilibrium thermodynamic treatments[2,3] to the relatively simple case of differential sorption.

The paper is organized as follows. The next section summarizes the phenomenology of viscoelastic diffusion, emphasizing the results found in part 1. Then, we summarize the linearized, one-dimensional (1D) constitutive laws for the liquid flux based on the thermodynamic theories by Durning and Tabor[2] and by Lustig et al.;[3] we find that the two developments give mathematically equivalent models. The common model is matched to the data from part 1 to extract transport properties (mutual binary diffusion coefficient, D_{12}; relaxation times, τ_i; ratio of mechanical modulus to osmotic modulus, $k_0 = D'/D$) for the PS–EB system at 40 °C as a function of composition in the concentrated polymer regime. Finally, these are compared with independent, published measurements using the free volume theory to correct the published values to our experimental conditions.

Background

Experimental Results. Differential Sorption Experiments. In the sorption method, a thin film of the mixture of depth l is initially equilibrated with a reservoir of fluid (typically vapor) at activity $a = a^-$. At time $t = 0$ the activity in the reservoir is incremented to a^+. The system relieves the resulting osmotic imbalance by mass transfer of fluid from the reservoir to the mixture; the dynamics are controlled by mutual diffusion within the film. One monitors the process by tracking the mass of the film as a function of time. Consider the linear perturbation limit of this experiment, commonly referred to as differential sorption. Here one applies a vanishingly small increment in a, i.e., $\delta a \equiv a^+ - a^- \to 0$; the corresponding increment in the mixture's equilibrium fluid weight fraction, $\delta w_1 \equiv w_1^+ - w_1^-$, also becomes vanishingly small. Consequently, when modeling this limit, one can linearize the governing field equations and boundary conditions with respect to the composition distribution. In one dimension, this limit offers a simple situation for testing a dynamic model against experiment.

Phenomenology of Linear Viscoelastic Diffusion. In part 1, we reported new differential sorption data on the poly(styrene) (PS)/ethylbenzene (EB) system. The sorptions were carried out at 40 °C on a thin (5 μm) film of monodisperse PS ($M_n \simeq 305\,000$) using the smallest possible increments in EB

* To whom correspondence should be addressed.
† Current address: Designed Thermoplastics Research, Dow Chemical Co., Midland, MI 48667.
® Abstract published in *Advance ACS Abstracts,* November 15, 1994.

0024-9297/94/2227-7630$04.50/0

activity. The effort supplied a series of good quality EB weight-uptake curves (i.e., plots of M_t/M_∞ versus $t^{1/2}$, where M_t means the mass of EB absorbed by the film at time t while M_∞ means the value of M_t for $t \to \infty$) near the linear perturbation limit as a function of the mean EB weight fraction for the sorption, $\langle w_1 \rangle$. The range of $\langle w_1 \rangle$ explored, $0.03 < \langle w_1 \rangle < 0.15$, includes the composition where the glass transition temperature, T_g, is depressed to the experimental temperature ($w_1 \simeq 0.10$); in other words, the range of compositions probed spanned the glass transition from below T_g (for $\langle w_1 \rangle < 0.10$) to above T_g (for $\langle w_1 \rangle > 0.10$).

The fluid weight-uptake kinetics showed distinctive viscoelastic features which changed systematically with increasing $\langle w_1 \rangle$. For the range $0.03 < \langle w_1 \rangle < 0.09$, in the glass state, the weight uptake curves were "two-stage", in which the uptake first increases as predicted by Fick's laws (linear with $t^{1/2}$), then levels, and finally relaxes in a second stage to the true equilibrium value over a relatively long time scale. At $\langle w_1 \rangle \simeq 0.095$, where T_g occurs, the time scale for the sorption process fell dramatically. The weight-uptake curves above this composition, in the range $0.10 < \langle w_1 \rangle < 0.12$, also showed viscoelasticity, although their shape changed dramatically. Here, the uptake plots initially show upward curvature, giving the plot an S or sigmoidal shape initially. Interestingly, a second, long-time-scale relaxation appears to affect the sorption data in this regime: The uptake plots relax at last 3–5% to final equilibium very slowly after the initial S-shaped portion (hence the term pseudosigmoid in ref 1 for the shape). At the highest EB contents probed, for $\langle w_1 \rangle > 0.12$, the uptake curves appeared to change to the ordinary Fickian response.

In part 1, these results were compared with a diffusion Deborah number correlation. A diffusion Deborah number, $(\mathrm{DEB})_\mathrm{D}$, is defined by

$$(\mathrm{DEB})_\mathrm{D} = \tau D_{12}/l^2 \tag{1}$$

where τ is a characteristic molecular relaxation time for the mixture, D_{12} is the binary mutual diffusion coefficient of the mixture, and l is the diffusion path length. $(\mathrm{DEB})_\mathrm{D}$ gives the ratio of a molecular relaxation time to the time for unsteady mutual diffusion. When this ratio is $\sim O(1)$, the molecular relaxation phenomena characterized by τ have the same time scale as the diffusion process and a viscoelastic response is anticipated in diffusion experiments.

We applied the method prescribed by Vrentas and Duda[16,17] to calculate $(\mathrm{DEB})_\mathrm{D}$ in the PS–EB system assuming τ is the terminal relaxation time of the linear viscoelastic mechanical spectrum. The calculations predict that viscoelastic diffusion should appear in the range $0.07 < \langle w_1 \rangle < 0.12$. This suggests that the terminal relaxation process (i.e, disentanglement) is involved in viscoelastic diffusion in this system at the upper end of the EB concentration range studied. That viscoelastic effects are also seen at $\langle w_1 \rangle$ as low as 0.03 suggests that relaxation processes with time scales much shorter than the terminal time also play an important role at low EB compositions.

The foregoing phenomenology pertains only to the linear perturbation limit of 1D sorption. Sorption experiments employing large increments in a manifest a much more complex variety of behaviors, including nonlinear ordinary diffusion,[18] "anomalous" diffusion,[19] "Case II" transport,[20] "super Case II" transport,[21] sorption overshoots,[22] and swelling fracture.[23] The observed diversity reflects the added complexity of nonlinearities from severe physical property changes with composition and, in some cases, deviations from a purely one-dimensional process.

Theoretical Results. The diffusion Deborah number correlation indicates that viscoelastic diffusion results from a coupling between the mass transfer and the viscoelastic response of the mixture. In what follows we summarize relevant results from two theories[2,3] using thermodynamic principles to account for this coupling.

Kinematics and Balance Laws for 1D Sorption. For 1D sorption (Figure 1), where both the polymer and fluid move only along the direction normal to the film plane, the composition completely determines the polymer deformation. (Strictly speaking, this is only true if one ignores the small volume change on mixing.) If the stress in the mixture is determined by the polymer deformation history, then the stress can be expressed in terms of the history of composition in the 1D case. Consequently, even if the diffusion flux depends explicitly on the stress distribution, as it does in several modern developments, one does not need to consider the force balance on the mixture for the 1D sorption problem; the continuity equations alone suffice.

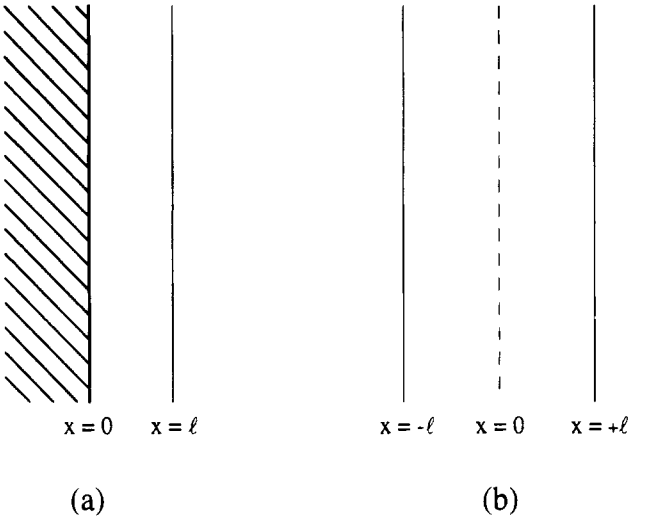

Figure 1. Schematic of the one-dimensional sorption problem.

In the Cartesian material coordinates,[24] fluid continuity is

$$\left(\frac{\partial C}{\partial t}\right)_\mathrm{X} = -\frac{\partial}{\partial X} J_\mathrm{X} \tag{2}$$

Here $C = \varrho_1/\varrho_2\hat{V}_2$ is the fluid mass per unit polymer volume and J_X is the diffusion flux of fluid along X relative to the polymer. All that one needs in addition in order to model the fluid concentration distribution, $C(X,t)$, and therefore the fluid weight-uptake kinetics during sorption, is an expression for J_X in terms of the concentration field and sufficient boundary and initial conditions on C.

For ordinary diffusion, Fick's law applies

$$J_\mathrm{X} = -D\frac{\partial C}{\partial X} \tag{3}$$

where D is the polymer material diffusion coefficient,[24] related to the binary mutual diffusion coefficient, D_{12}, by

$$D = (\varrho_2\hat{V}_2)^2 D_{12}$$

Viscoelastic Constitutive Laws for J_X. Boundary Conditions. Durning and Tabor[2] (DT) derived a viscoelastic law for J_X based the nonequilibrium thermodynamics of materials with memory.[25] A synopsis of the development appears in Appendix A. Equations 24 and 28 of Appendix A are the main results. The latter prescribes the effect of memory on the fluid's chemical potential, while the former gives the flux as proportional to the gradient of the potential. Combining the two gives for the flux in 1D

$$J_\mathrm{X} = -D\frac{\partial C}{\partial X} - D'\frac{\partial}{\partial X} g(C)\int^t \varphi(t-t',C')\frac{\partial C'}{\partial t'}\,\mathrm{d}t' \tag{4}$$

where $g(C)$ means $G(C)/G_0$, with $G(C)$ being the instantaneous shear modulus of the mixture and $G_0 = G(C=0)$. Also,

$$D' = D\frac{G_0 V_1}{RT(-\partial f/\partial \ln w_2)}\varrho\hat{V}_1 \tag{5}$$

where V_1 means the molar volume of the fluid, ϱ means the density of the mixture, and RTf/M_1 corresponds to the fluid's

thermostatic (i.e., equilibrium) chemical potential. Note that D'/D gives the ratio of the instantaneous mechanical modulus of the dry material, G_0, to the bulk osmotic modulus $-RT(\partial f/\partial \ln w_2)/V_1$.

Regarding the boundary conditions, at phase interfaces DT assumed that the fluid chemical potential (eq 28 in Appendix A) is continuous. For vapor sorption, this leads to a surface boundary condition expressed conveniently in terms of the external reservoir activity, $a(t)$:

$$\ln a(t) = f + Q\int^t \varphi(t-t',C')\frac{\partial C'}{\partial t'}\,dt' \qquad (6)$$

where $Q = (GV_1/RT)\varrho_2\hat{V}_2\hat{V}_1$.

Lustig et al.[3,27] derived an expression for the fluid flux from the thermodynamic theory of mixtures;[28] Appendix B summarizes the main results. The flux is related to the difference of "partial" stress tensors for the fluid and the polymer in the mixture, which characterize each component's contribution to the total stress. The tensorial result from the DT development differs from Lustig's (cf. eq 23 in Appendix A versus eqs 32 and 33 in Appendix B). However, for "simple mixtures" (see Appendix B and ref 3) and 1D transport, Lustig's tensorial result reduces to the same form derived by DT (cf. eqs 4 and 5 versus eqs 34–38 in Appendix B); the only differences between the two developments in this case are the interpretations of D', $\varphi(t-t',C')$, and $g(C)$ (see Appendix B).

Lustig et al. also discuss boundary conditions at phase interfaces. The key relation, a jump linear momentum balance, is, in general, distinct from matching the fluid chemical potential at phase boundaries (see Appendix C). However, for the 1D sorption problem the jump momentum blance has the same mathematical structure as eq 6. In the analysis which follows we adopt eq 6.

Linearization. Consider the simplifications implied for a linear perturbation experiment. In eqs 3, 4, and 6, D, D', φ, f, and Q all depend on C (this dependence is **very** strong for D,[29] D', and φ). So, a mathematical model for one-dimensional sorption based on these relations is, in general, a nonlinear initial value problem. However, for a linear perturbation experiment, the concentration field has the form

$$C(X,t) = C^- + \delta C(X,t); \qquad |\delta C(X,t)/C^-| \ll 1 \qquad (7)$$

and the reservoir activity is controlled so that

$$a(t) = a^- + \delta a(t); \qquad |\delta a(t)/a^-| \ll 1 \qquad (8)$$

which permit linearization of eqs 3, 4, and 6 with respect to C and a.

Denote the value of any composition-dependent property p at C^- by p^-; the linearized flux expressions have the same form as eqs 3 and 4 but with the replacements $C(X,t) \rightarrow \delta C(X,t)$ and $p(C) \rightarrow p^- = \text{const}$. When eq 6 is linearized, the resulting expression is

$$\frac{\delta a(t)}{a^-} = \left(\frac{\partial f}{\partial C}\right)^- \delta C + Q^-\int^t \varphi^-(t-t')\frac{\partial \delta C'}{\partial t'}\,dt' \qquad (9)$$

Mathematical Models of Differential Sorption. The incremental fluid concentration during differential sorption, $\delta C(X,t)$, obeys the diffusion equation obtained by combining fluid continuity (eqs 2 and 7) with an expression for the flux (the linearized form of either eq 3 or eq 4). In Appendix D, we derive the viscoelastic model for $\delta C(X,t)$ using the generalized Maxwell model as a robust form for the relaxation function, φ. The Appendix also summarizes a convenient method of calculating the measurable relative weight uptake, ω.

Quantitative Comparison between Theory and Experiment

Summary of Sorption Runs from Part 1. Table 1 lists the differential sorption experiments reported in part 1 in the order of ascending mean ethylbenzene content, $\langle w_1\rangle$. The pressure increment for the run, the state of the mixture during the run (glass or liquid), and the shape of the ethylbenzene weight-uptake curve are also given for each case. The state of the mixture was determined from the dilatometrically measured glass transition temperatures of poly(styrene)/ethylbenzene mixtures, as discussed in part 1. Not all of the runs listed are analyzed subsequently. In particular, runs R-1 and R-2 are not analyzed since the data were not of the best quality. Also, as indicated in the table, the runs in several sets had essentially the same mean ethylbenzene content; these groups of runs were shown in part 1 to be superimposable. In these cases only one run of the set is analyzed in detail below.

Table 1. Summary of Differential Sorption Runs Reported in Part 1[a]

run	$\langle\omega_1\rangle$	pressure increment (Torr)	state	weight uptake
R-1[b]	0.0036	0.0–1.2	glass	
R-2[b]	0.0099	1.2–2.9	glass	
R-3	0.0276	2.9–4.0	glass	two-stage
R-4	0.0600	4.0–4.9	glass	two-stage
R-5[c]	0.0837	4.9-5.9	glass	two-stage
R-6[c]	0.0878	5.9-6.6	glass	two stage
R-9	0.0905	6.3–6.6	glass/liquid	two-stage
R-15[d]	0.1017	7.4–7.5	liquid	pseudo-sigmoid
R-10[d]	0.1023	6.6–7.0	liquid	pseudo-sigmoid
R-7[d]	0.1026	6.6–7.2	liquid	pseudo-sigmoid
R-13	0.1068	7.0–7.1	liquid	pseudo-sigmoid
R-11[e]	0.1101	7.0–7.3	liquid	pseudo-sigmoid
R-14[e]	0.1138	7.1–7.3	liquid	pseudo-sigmoid
R-16[e]	0.1156	7.5–8.0	liquid	pseudo-sigmoid
R-12[f]	0.1181	7.3–7.5	liquid	Fickian
R-8[f]	0.1185	7.2–7.6	liquid	Fickian
R-17	0.1308	8.0–8.3	liquid	Fickian
R-18	0.1425	8.3–8.6	liquid	Fickian

[a] All runs were on a 5-μm-thick PS film (MW = 305 000; PDI = 1.05) at 40 °C. [b] Data for these runs were not of good quality. [c–f] Runs with common superscripts gave essentially identical weight-uptake curves.

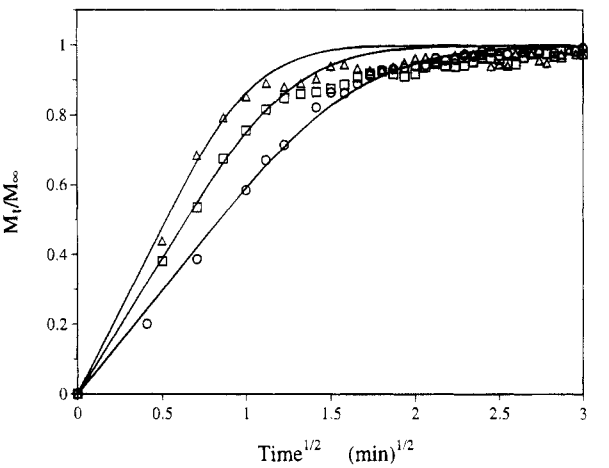

Figure 2. Plot of M_t/M_∞ vs $t^{1/2}$ for runs R-12 (○) ($\langle w_1\rangle$ = 0.1181), R-17 (□) ($\langle w_1\rangle$ = 0.1308), and R-18 (△) ($\langle w_1\rangle$ = 0.1425); all three uptake curves show Fickian characteristics. The solid lines show the predictions of Fick's law based on the diffusion constants in Table 2.

Analysis of Classical Sorption Data. As shown in Figure 2, sorption data from runs R-12, R-17, and R-18 appear to obey the classical theory for 1D transport in a thin film, viz., the relative weight uptakes increase linearly with $t^{1/2}$ initially, grow increasingly concave to the $t^{1/2}$ axis as time increases, and appear to achieve the ultimate, equilibrium values without a protracted relaxation. This behavior is expected since these runs were carried out at the highest mean ethylbenzene (EB)

Table 2. Analysis of Classical Sorption Curves

run	$\langle w_1 \rangle$	D (cm^2/s)[a]
R-12	0.1181	2.89×10^{-10}
R-17	0.1308	4.95×10^{-10}
R-18	0.1425	7.48×10^{-10}

[a] Calculated by fitting the Fick's law solution to the data, as shown in Figure 2 with $l = 2.5 \times 10^{-4}$ cm.

weight fractions ($\langle w_1 \rangle$) accessible in our equipment, which correspond to liquid-state conditions (see Table 1), i.e., significantly above the effective glass transition temperature in the PS–EB system. Consequently, we analyzed these data for the polymer–material diffusion coefficients, D, using the classical theory, as follows.

A dimensionless plot was prepared of the standard eigenfunction solution for M_t/M_∞ vs $(Dt/l^2)^{1/2}$ for sorption in a thin film according to Fick's law. Then, each set of data were superimposed on this plot after guessing a value of $(D/l^2)^{1/2}$. After finding a value which gave a very good visual match between the prediction and the data (Figure 2), D was calculated from the known value of l ($\cong$2.5 μm). Table 2 summarizes the results from this analysis. In all three cases, $D \sim O(10^{-10}$ cm^2/s), which is a reasonable value for a fluid of molecular weight $M_1 \sim O(100$ g/gmol) in an amorphous polymer slightly above its glass transition temperature.[32] As is typical of polymer–solvent systems, D increases with fluid content. Comparison of D and their composition dependence with previously published values for the PS–EB system is given subsequently.

Before analyzing the viscoelastic two-stage and pseudosigmoidal sorption curves found at lower EB contents, the reader should note that the data in Figure 2 actually do show a weak deviation from the classical predictions. Note that the theory overshoots the data at long times in all three cases, suggesting a long-time-scale relaxation process affects the data. This deviation is remnant of the more obvious viscoelastic behavior seen at slightly lower EB fractions than for run R-12 (at these conditions pseudosigmoidal uptake curves were found, which clearly display a protracted relaxation to equilibrium at long times; see Table 1).

Analysis of Viscoelastic Sorption Data. In the majority of our differential sorption runs, the classical predictions are not obeyed. In these cases, eqs 48–52 of Appendix D were fit to the data by systematic manipulation of the transport properties as follows. First, a dimensionless weight-uptake curve is prepared with the same shape as the data by trial manipulation of the dimensionless parameters k_0 and k_i (see eq 48 of Appendix D). The data are then scaled along the abscissa by a proper choice of D (see eqs 47 of Appendix D) in order to match the dimensionless prediction. This procedure supplies, with a minimum of effort, a set of transport coefficients giving a very good fit to the data, although not necessarily optimized in the least-squares sense.

Figures 3–9 show M_t/M_∞ versus $(Dt/l^2)^{1/2}$ according to experiment and theory for the majority of runs listed in Table 1 as showing viscoelastic effects. For the two-stage sorption curves (see Table 1 and Figures 3–6), a single Maxwell element ($n = 1$ in eqs 40–42) was used to model the data; adding additional Maxwell elements **did not** produce a better fit but, in fact, degraded the model's representation of the data. In contrast, for the pseudosigmoidal sorption curves (Table 1 and Figures 7–9), which show a slow, long-time-scale relaxation to the final equilibrium value, two Maxwell elements in parallel ($n = 2$ in eqs 40–42) were used since the additional element did enable a better fit, to the long-time portion of the data. These features are discussed in more detail below.

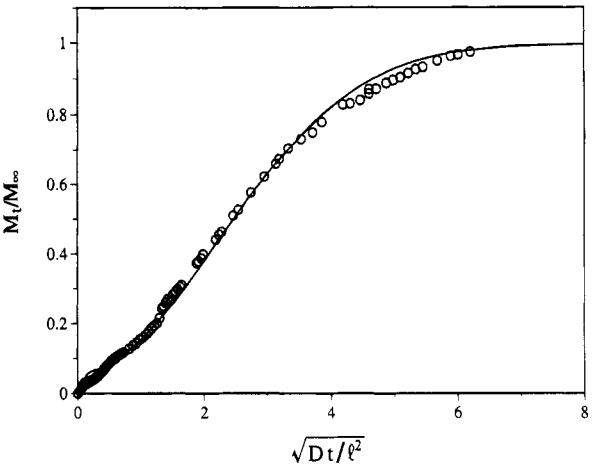

Figure 3. Plot of M_t/M_∞ vs $(Dt/l^2)^{1/2}$ for run R-3 showing the data and the predictions with $k_0 = D'/D = 30$ and $k_1 = 0.3$, using $D = 8.8 \times 10^{-13}$ cm^2/s to scale the abscissa.

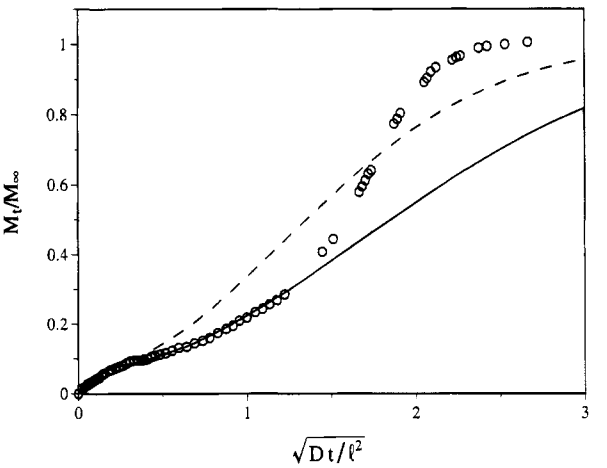

Figure 4. Plot of M_t/M_∞ vs $(Dt/l^2)^{1/2}$ for run R-4 showing the data and the predictions with $k_0 = D'/D = 25$ and $k_1 = 0.2$ (solid line) and with $k_0 = D'/D = 25$ and $k_1 = 0.1$ (dashed line), both using $D = 5.0 \times 10^{-13}$ cm^2/s to scale the abscissa.

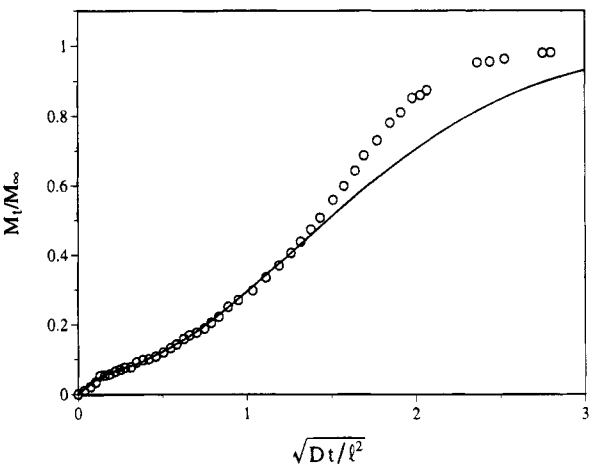

Figure 5. Plot of M_t/M_∞ vs $(Dt/l^2)^{1/2}$ for run R-5 showing the data and the predictions with $k_0 = D'/D = 30$ and $k_1 = 0.1$, using $D = 1.4 \times 10^{-12}$ cm^2/s to scale the abscissa.

Figure 3 shows a plot of M_t/M_∞ versus $(Dt/l^2)^{1/2}$ for run R-3 ($\langle w_1 \rangle = 0.0276$). The solid line shows the theoretical prediction using the dimensionless parameters $k_0 = D'/D = 30$ and $k_1 = 0.3$, which gives a sorption

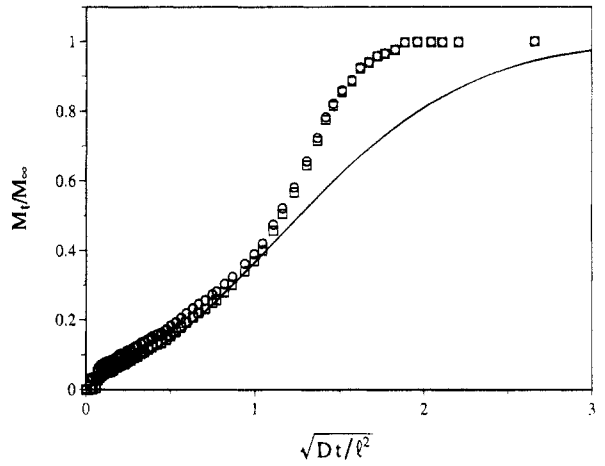

Figure 6. Plot of M_t/M_∞ vs $(Dt/l^2)^{1/2}$ for run R-9 showing the raw data (○) and the adjusted data (□), along with predictions with $k_0 = D'/D = 30$ and $k_1 = 0.07$, using $D = 1.8 \times 10^{-12}$ cm²/s to scale the abscissa.

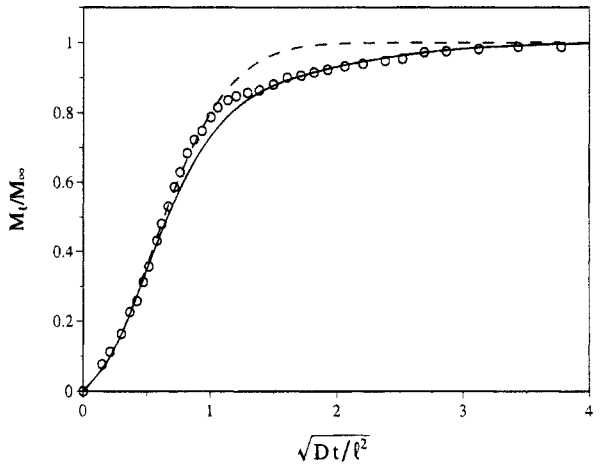

Figure 7. Plot of M_t/M_∞ vs $(Dt/l^2)^{1/2}$ for run R-7 showing the data and the predictions for two Maxwell elements with $k_0 = D'/D = 30$, $k_1 = 0.01$, $k_2 = 3.0$, and $g_1 = 0.994$ (solid line) and for a single Maxwell element with $k_0 = D'/D = 30$ and $k_1 = 0.01$ (dashed line), both using $D = 2.3 \times 10^{-11}$ cm²/s to scale the abscissa.

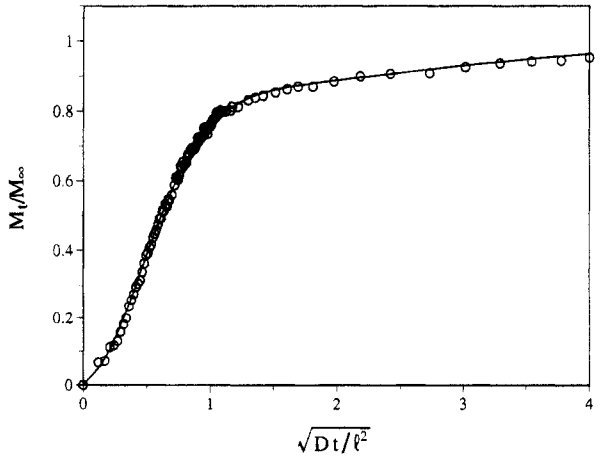

Figure 8. Plot of M_t/M_∞ vs $(Dt/l^2)^{1/2}$ for run R-13 showing the data and the predictions for two Maxwell elements with $k_0 = D'/D = 30$, $k_1 = 0.007$, $k_2 = 9.0$, and $g_1 = 0.994$, using $D = 6.0 \times 10^{-11}$ cm²/s to scale the abscissa.

curve with the correct shape. Using the dry polymer film half-thickness, $l = 2.5 \times 10^{-4}$ cm, a (polymer material) diffusion coefficient $D = 8.8 \times 10^{-13}$ cm²/s was needed to scale the $t^{1/2}$ axis so as to match the experiment with theory. The resulting agreement between

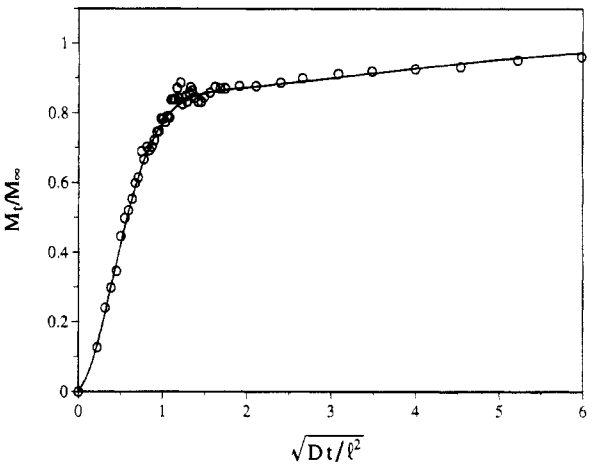

Figure 9. Plot of M_t/M_∞ vs $(Dt/l^2)^{1/2}$ for run R-14 showing the data and the predictions for two Maxwell elements with $k_0 = D'/D = 30$, $k_1 = 0.005$, $k_2 = 18.0$, and $g_1 = 0.994$, using $D = 2.1 \times 10^{-10}$ cm²/s to scale the abscissa.

the data and the prediction is quite good over the entire time scale. However, for the majority of the two-stage uptake curves, the theoretical representation of the data was not as good as for this case.

Figure 4 shows M_t/M_∞ versus $(Dt/l^2)^{1/2}$ for run R-4 ($\langle w_1 \rangle = 0.0600$) along with a dimensionless prediction using $k_0 = 25$ and $k_1 = 0.2$. Here, $D = 5.0 \times 10^{-13}$ cm²/s was used to scale the time. For times shorter than $(Dt/l^2)^{1/2} \simeq 1.25$, the theoretical representation of the data is excellent; however, for longer times the prediction badly underestimates the uptake data. For this run and for the remaining runs showing two-stage weight uptake (Figures 5 and 6), we had difficulty representing the data over the entire time scale with a single relaxation time. In each of these cases, the dimensionless parameters for the predictions (solid lines in the figures) were chosen to match the uptake data at short times; we believe this results in the most accurate values of the transport properties for the interval in question, for the reasons discussed below. It is, of course, possible to choose a different set of parameters in these cases which would produce a better long-time representation while compromising the fit at short times (see, for example, the fit of run R-4 in Figure 4 using $k_0 = 25$ and $k_1 = 0.1$ (dashed line)).

We emphasize that including additional Maxwell elements **cannot** improve the representations of the two-stage data in Figures 4–6. This is easy to appreciate. The solid lines in Figures 4–6 represent the short time response very well, so the addition of elements with shorter relaxation times degrades the short time scale predictions; the addition of elements with longer relaxation times produces an even slower approach to equilibrium than already predicted, which would degrade the long time predictions.

We believe the main reason the linear theory fails to represent the two-stage data in Figures 4–7 over the whole sorption time scale is that the experimental responses in these cases are mildly nonlinear. This is suggested by the fact that the ethylbenzene weight fraction interval for run R-4, δw_1, is relatively large ($\simeq$0.037) and clearly violates a criterion for linearity in the PS–EB system under the conditions of interest, that $\delta w_1 \leq 0.01$. (This bound on δw_1 is calculated from the Vrentas–Duda free volume theory and the requirement that the mutual diffusion coefficient remain within 10% of its initial value during a sorption.) The very strong effect of fluid content on mechanical relaxation times

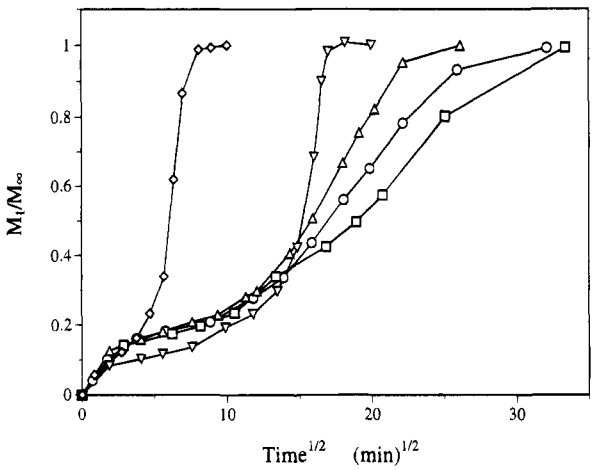

Figure 10. Differential sorption data[33] for polystyrene/benzene at 25 °C where the initial pressure is fixed at 47.5 Torr and the final pressures are 53 (□), 55 (○), 56 (△), 59 (▽), and 62 Torr (◇).

suggests the main consequence of a weak nonlinearity: The relaxation time governing the second stage decreases as the sorption process proceeds, i.e., as the average fluid content in the film increases, thereby accelerating the uptake at long times. This would produce exaggerated upward curvature of the data in the second stage portion of the plot compared to that expected for a purely linear response, causing positive deviations of the data from the linear theory at long times, exactly like those seen in Figure 4. The experiments by Odani et al.[33] support this interpretation in that they confirm the influence of weak nonlinearities in differential sorption. Odani et al. explored the effect of progressively increasing δw_1 in a series of differential sorptions with a fixed initial fluid content, w_1^-. Figure 10 shows their data for progressively increasing pressure intervals (and, therefore, progressively increasing δw_1) in the system polystyrene/benzene at 25 °C; the data show that the first stage is virtually unaffected by the magnitude of the concentration increment but that the second stage is accelerated as δw_1 increases.

This discussion implies that better representations of our two-stage data by the linear theory should be obtained for experiments with smaller pressure increments; the analysis of our two-stage curves verifies this. The ethylbenzene weight fraction interval for run R-4 is the largest among the 18 runs carried out, and the theoretical representation by the linear theory is the worst for this case (compare Figure 4 with Figures 3, 5 and 6).

Figure 5 shows M_t/M_∞ versus $(Dt/l^2)^{1/2}$ for run R-5 ($\langle w_1 \rangle = 0.0837$) along with the dimensionless predictions for $k_0 = 30$ and $k_1 = 0.01$. Here $D = 1.4 \times 10^{-12}$ cm^2/s has been used to scale time. Since runs R-5 and R-6 were nearly coincident (see part 1), this fit applies to run R-6 as well. As for run R-4, the prediction matches the data very well at short times; however, for $(Dt/l^2)^{1/2} \geq 1.4$ the data approach equilibrium more rapidly than predicted. In this case the deviation between the data and the prediction is smaller than for R-4, which is consistent with the ethylbenzene weight fraction interval in R-5 being less than half of that in run R-4 (see Table 1). Clearly, this run is closer to the linear limit than R-4.

For run R-9 ($\langle w_1 \rangle = 0.0905$), the sorption isotherm indicated that the initial ethylbenzene content was suspiciously low and, therefore, might not correspond to the true equilibrium value at the initial ethylbenzene pressure for this run. Consequently, we plotted M_t/M_∞ versus $(Dt/l^2)^{1/2}$ for run R-9 (Figure 6) using both the original data (open circles) and also considering the second data point as the initial condition (open squares). The adjusted data lie only slightly below the original data. In both cases, $D = 1.8 \times 10^{-12}$ cm^2/s has been used to scale the time. The solid line indicates the dimensionless prediction for $k_0 = 30$ and $k_1 = 0.07$. The fit to the adjusted data is very good up to $(Dt/l^2)^{1/2} \simeq 1$. As in the previous two plots, the prediction underestimates the uptake during the second stage.

Figure 7 shows the analysis of the first of the pseudosigmoidal sorption curves; M_t/M_∞ is plotted against $(Dt/l^2)^{1/2}$ for run R-7 ($\langle w_1 \rangle = 0.1026$). The solid line shows the prediction using two Maxwell elements, with $k_0 = 30$, $k_1 = 0.01$, $k_2 = 3.0$, and $g_1 = 0.994$. Here, $D = 2.3 \times 10^{-11}$ cm^2/s has been used to scale the time axis. From the reproducibility of runs around this weight fraction, demonstrated in part 1, this fit applies also to runs R-10 and R-15. Overall, the correspondence between the data and the prediction is very good although the prediction does slightly underestimate the data toward the end of the first relaxation process (i.e., at $(Dt/l^2)^{1/2} \simeq 1$). This deviation might be the result of a weak nonlinearity, since $\delta w_1 \simeq 0.016 > 0.01$ for this run.

For this, and all other pseudosigmoidal uptake curves, a fit based on two Maxwell elements gave a better representation than that based on just one (e.g., dashed line in Figure 7). With only one relaxation time, the long time data are overestimated after properly fitting the short time response. Adding a second element with a longer relaxation time and a smaller modulus retards the long time prediction and improves the agreement with data at long times. This situation differs qualitatively from that discussed above in connection with the two-stage uptake curves. In that case the long time predictions underestimated the data, which cannot be corrected by adding additional elements.

Figure 8 shows M_t/M_∞ versus $(Dt/l^2)^{1/2}$ for run R-13 ($\langle w_1 \rangle = 0.1068$), where $D = 6.0 \times 10^{-11}$ cm^2/s has been used to scale the time, along with the two-element prediction using $k_0 = 30$, $k_1 = 0.007$, $k_2 = 9.0$, and $g_1 = 0.994$. There is virtually no deviation between the data and prediction over the entire time scale. In fact, this run can probably be considered truly linear since $\delta w_1 \simeq 0.01$, one of the smallest values achieved in the study.

Figure 9 shows a similar situation, with data from run R-14 ($\langle w_1 \rangle = 0.1138$) plotted along with the prediction using $D = 2.1 \times 10^{-10}$ cm^2/s to scale time and $k_0 = 30$, $k_1 = 0.005$, $k_2 = 18.0$, and $g_1 = 0.994$ to achieve the correct shape. As demonstrated in part 1, the data for runs R-11, R-14, and R-16 are nearly coincident, so this fit applies for all three. Note that the data and the theory match extremely well over the whole range of time in this case; this is consistent with the very small concentration interval used, $\delta w_1 \simeq 0.006$, which ensures that the assumption of linear response is a good approximation.

Analysis of Transport Properties

Table 3 summarizes the results of the analysis in the previous section. In what follows, the transport properties calculated from these, and their trends with composition, are compared with published results. In particular, we consider the diffusion coefficients D, the relaxation times τ_i, the ratios D'/D, and the moduli g_i. The comparisons for the first two involve the correction

Table 3. Parameters Calculated from Viscoelastic Sorption Data

run	$\langle w_1 \rangle$	k_0	k_1	k_2	g_1	D (cm²/s)
R-3	0.0276	30	0.3			8.8×10^{-13}
R-4	0.0600	25	0.2			5.0×10^{-13}
R-5	0.0837	30	0.1			1.4×10^{-12}
R-9	0.0905	30	0.07			1.8×10^{-12}
R-7	0.1026	30	0.01	3.0	0.994	2.3×10^{-11}
R-13	0.1068	30	0.007	9.0	0.994	6.0×10^{-11}
R-14	0.1138	30	0.005	18.0	0.994	2.1×10^{-10}

of published values for the differences in temperature and composition between our study and the reference studies using the Vrentas–Duda free volume theory.

Diffusion Coefficient. Tables 2 and 3 list the polymer material diffusion coefficients obtained from our data. One sees that, up to an EB weight fraction of $\langle w_1 \rangle \simeq 0.09$, D remains practically constant at $\sim O(10^{-12}$ cm²/s). At higher EB contents, D increases monotonically with $\langle w_1 \rangle$.

Vrentas and Duda[4,5] developed a free volume theory accurately describing the temperature and composition dependence of diffusion coefficients in polymer–fluid mixtures over a broad range of conditions in the liquid state. In ref 34, they expressed the binary mutual diffusion coefficient, D_{12}, as

$$D_{12} = D_1 G \tag{10}$$

where D_1 is the self-diffusion coefficient of the fluid in the mixture, obeying

$$D_1 = D_{01} \exp[-(w_1 \hat{V}_1^* + w_2 \xi \hat{V}_2^*)/(\hat{V}_{FH}/\gamma)] \tag{11}$$

Here D_{01} depends on temperature

$$D_{01} = D_0 \exp(-E/RT) \tag{12}$$

with D_0 and E being constants. E represents the average energy barrier for a stochastic jump of a mobile segment in the mixture. G is a thermodynamic factor, related to the mixture's osmotic modulus, given in the Flory–Huggins theory as

$$G = (1 - \varrho_1 \hat{V}_1)^2 (1 - 2\chi \varrho_1 \hat{V}_1) \tag{13}$$

with χ being the Flory–Huggins interaction parameter. The $\hat{V}_i^*$ are hard-core specific volumes corresponding to the minimum hole size enabling a stochastic jump of a mobile segment of species i, ξ gives the ratio of the fluid and polymer mobile jumping segment volumes, and $\hat{V}_{FH}/\gamma$ is the effective specific free volume enabling stochastic jumps. For mixtures in the liquid state (above the glass transition), Vrentas and Duda assumed that $\hat{V}_{FH}/\gamma$ is the mass fraction weighted sum of the pure-component values, $\hat{V}_{FHi}/\gamma$:

$$\hat{V}_{FH}/\gamma = w_1 \hat{V}_{FH1}/\gamma + w_2 \hat{V}_{FH2}/\gamma = w_1 (K_{21} + T - T_{g1})(K_{11}/\gamma) + w_2 (K_{22} + T - T_{g2})(K_{12}/\gamma) \tag{14}$$

Here, $K_{21} - T_{g1}$ and K_{11}/γ are free volume constants for the pure fluid, while $K_{22} - T_{g2}$ and K_{21}/γ are those for the pure polymer; these are, essentially, the WLF constants for the pure components. Of the parameters appearing in the theory, all but four, χ, D_0, E, and ξ, are determined from pure-component properties.

In part 1, we determined $\chi = 0.05$ from the sorption isotherm for PS/EB at 40 °C and, so, used this value in the evaluation of G (eq 13). Table 4 summarizes the remaining parameters used to compare our diffusion

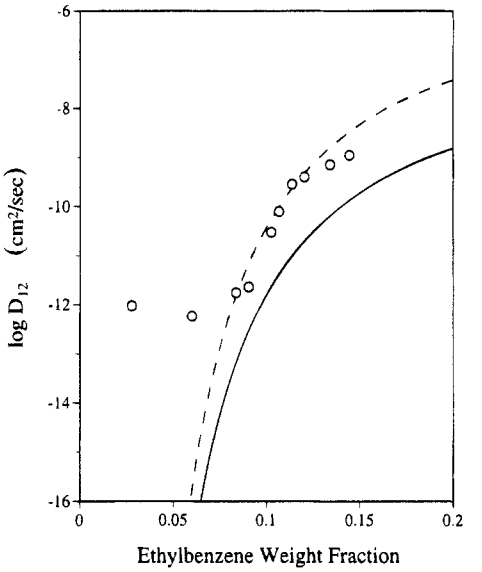

Figure 11. Plot of log D_{12} (cm²/s) vs w_1 showing the D_{12} extracted from viscoelastic sorption data and extrapolations of independently measured values via the liquid-state free volume theory. The solid line shows the free volume calculation with ξ and D_{01} determined by Duda et al;[34] the dashed line shows the calculation based on ξ and D_{01} from a fit of eq 11 to the self-diffusion data at 40 °C reported in ref 35.

Table 4. Parameters in the Vrentas–Duda Free Volume Theory

parameter	value	ref
χ	0.05	1
$\hat{V}_1^*$	0.946 (cm³/g)	34
$\hat{V}_2^*$	0.850 (cm³/g)	34
K_{11}/γ	2.05×10^{-3} (cm³/g K)	34
K_{12}/γ	5.82×10^{-4} (cm³/g K)	34
$K_{21} - T_{g1}$	−96.7 (K)	34
$K_{22} - T_{g2}$	−327 (K)	34
ξ	0.56	34
D_{01}	2.7×10^{-6} (cm²/s)	34
ξ	0.563	35
D_{01}	6.85×10^{-5} (cm²/s)	35

coefficients to the Vrentas–Duda theory. In one comparison, the constants $\hat{V}_i^*$, K_{ij}/γ, $K_{ij} - T_{gj}$, ξ, D_0, and E in eqs 10–14 are those reported by Duda et al.[34] for PS/EB; here the values of ξ, D_0, and E were fixed by fitting mutual diffusion from sorption data taken at high temperatures (115–180 °C), where viscoelastic effects are completely absent. In a second comparison, we used all the pure-component parameters reported in ref 34 but fixed ξ and D_{01} (=$D_0 \exp(-E/RT)$) by fitting eq 11 to the self-diffusion data reported by Zgadzai and Maklakov,[35,36] measured by NMR at 40 °C over the composition range $0.19 \leq w_1 \leq 0.60$.

Figure 11 shows the data, plotted as log D_{12} vs w_1, along with the values calculated from the free volume theory. The solid line shows the result using ξ, D_0, and E determined from the high-temperature sorption data reported in ref 34, while the dashed line shows the result when ξ and D_{01} are evaluated from the self-diffusion data reported in ref 35. In effect, Figure 11 directly compares diffusion coefficients extracted from our viscoelastic sorption data with those measured independently in the liquid state, where viscoelastic effects are absent.

The free volume calculation based on the high-temperature sorption data (solid line in Figure 11) shows the correct trend with composition for $w_1 \geq 0.09$, but it underestimates D_{12} over the entire concentration range; this is likely the result of an inaccurate extrapo-

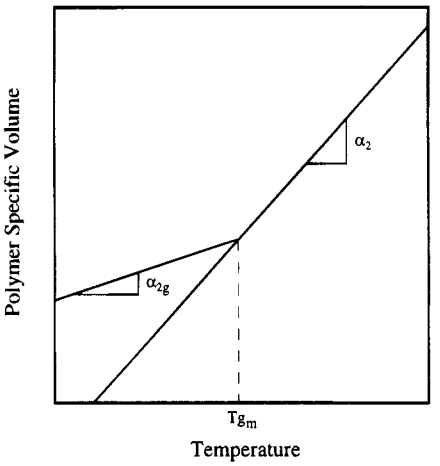

Figure 12. Schematic $\hat{V}_2$ vs T plot showing the thermal expansion coefficient of the equilibrium liquid, α_2, and the shift to a lower value, α_{2g}, below T_{gm}.

lation via the free volume theory of the high-temperature behavior analyzed in ref 34. This view is supported by the comparison based on the values of ξ and D_{01} determined from the self-diffusion data reported in ref 35 (dashed line in Figure 11), which were measured at conditions much closer to our experiments than those in ref 34. Here we find very good quantitative agreement with our data for $w_1 \geq 0.09$. For smaller w_1 the experimental D_{12} remain nearly constant, while the free volume theory predicts unrealistically small values as the pure polymer limit is approached.

From the calculation using D_{01} based on the self-diffusion data, the deviation between our data and the liquid-state free volume theory begins at a composition where we observed a dramatic change in the time scale for sorption and a shift from two-stage to pseudosigmoidal weight uptake curves (see Phenomenology of Linear Viscoelastic Diffusion). In part 1, we associated these sudden changes with glassification, i.e., the point where the glass transition temperature of the mixture, T_{gm}, is depressed to the experimental temperature. Indeed dilatometric measurements of T_{gm} in PS/EB mixtures provided direct support of this. Consequently, we associate the leveling of D vs w_1 in the left portion of Figure 11 with glassification.

To account for glassification in the free volume theory, we considered the modification proposed by Vrentas, Duda, and Ling.[6,7] They included "excess" free volume trapped below the glass transition; Figure 12 illustrates their idea with a schematic specific volume–temperature plot. Equation 14 assumes that the polymer's volumetric behavior below the glass transition is governed by the same thermal expansion coefficient controlling the equilibrium polymeric liquid, α_2. The modification accounts for the shift of the thermal expansion coefficient with decreasing temperature to a lower value, α_{2g}, at the glass transition (see Figure 12). The temperature where this shift occurs is T_{gm}. For concentrated polymer–fluid mixtures, T_{gm} can be represented[6,7]

$$T_{gm} = T_{g2} - Aw_1 \tag{15}$$

where T_{g2} is the glass transition temperature for the pure polymer and A is a constant which quantifies the plasticizing effect of the fluid. This relationship applies for PS/EB mixtures with $A = 647$ K, as demonstrated in part 1 (see Figure 8 in ref 1).

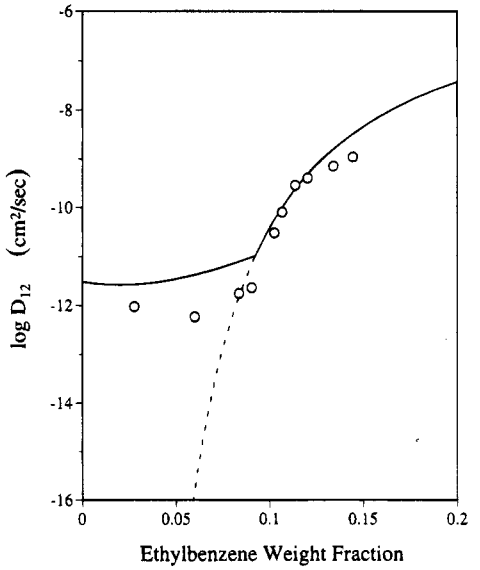

Figure 13. Plot of log D_{12} (cm²/s) vs w_1 showing the D_{12} extracted from viscoelastic sorption data and extrapolations of independently measured values via the free volume theory modified to account for trapped free volume below T_{gm}, as described in the text.

Table 5. Parameters for Free Volume Theory below the Glass Transition

parameter	value	ref
A	647 (K)	1
γ	0.595	17
$\hat{V}_2^o(T_{g2})$	0.9760 (cm³/g)	38
T_{g2}	373 (K)	39
α_2	5.5×10^{-4} (K^{-1})	37, 39
α_{2g}	1.8×10^{-4} (K^{-1})	37, 39

Now, the actual specific volume of the mixture below T_{gm} contracts less with temperature than above T_{gm}. Vrentas et al.[6,7] suggested that the difference between the actual and equilibrium specific volumes is extra free volume and that an additional term be added to eq 14 to account for the difference. This excess specific hole free volume, $\hat{V}_{FH}^E$, was expressed as

$$\frac{\hat{V}_{FH}^E}{\gamma} = \frac{w_2\hat{V}_2^o(T_{g2})}{\gamma}(1 - Aw_1\alpha_2)(T - T_{g2} + Aw_1)(\alpha_{2g} - \alpha_2) \tag{16}$$

where $\hat{V}_2^o(T_{g2})$ is the equilibrium specific volume of the polymer at its glass transition temperature. The parameters needed to apply eq 16 appear in Table 5; these were determined from independent experimental measurements reported in the literature.

Figure 13 shows log D vs w_1 with the prediction according to eq 14 at compositions where the mixture is above the glass transition ($w_1 \geq 0.09$) and according to eq 14 with eq 16 added to $\hat{V}_{FH}/\gamma$ for compositions where the mixture is below T_{gm}. The free volume extrapolation below T_{gm} shows reasonable qualitative agreement with the data, considering that none of the parameters in Table 5 were adjusted to fit the data. This calculation lends strong support for both the free volume theory for conditions below T_{gm} and the (linearized) theory for viscoelastic diffusion.

Relaxation Times. Table 3 summarizes the diffusion Deborah numbers, k_1 and k_2, determined by analyzing the viscoelastic weight-uptake curves. We find that k_1 decreases monotonically with increasing ethylbenzene content, while k_2 increases over the narrow

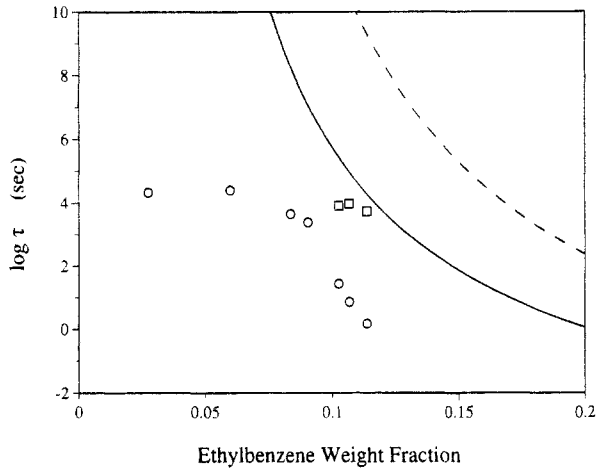

Figure 14. Plot of log τ (s) vs w_1 showing the relaxation times τ_1 (○) and τ_2 (□) compared with the terminal time shifted to our experimental conditions via free volume theory from data by Akovali[10] (solid line) and by Richards and Prud'homme[11] (dashed line).

Table 6. Relaxation Times Calculated from Viscoelastic Sorption Data

run	$\langle w_1 \rangle$	τ_1 (s)	τ_2 (s)
R-3	0.0276	21 300	
R-4	0.0600	25 000	
R-5	0.0837	4460	
R-9	0.0905	2430	
R-7	0.1026	27.2	8152
R-13	0.1068	7.29	9375
R-14	0.1138	1.49	5357

composition range where it could be determined. The trend in k_1 with w_1 agrees with that predicted for the diffusion Deborah number by Vrentas et al. using the free volume theory[16,17] (see also part 1). The trend in k_2 goes against the free volume predictions, but it must be admitted that the k_2 could not be determined very precisely and there are only three values, so the tabulated trend should be viewed with caution.

With the experimentally determined diffusion coefficients, D, and the initial film half-thickness, l, relaxation times were calculated from the k_i using eq 49; these are summarized in Table 6. In their calculation of Deborah numbers, Vrentas et al.[16,17] assumed the relaxation time to be the terminal time for the mixture, implying that disentanglement is the dominant molecular relaxation process involved in viscoelastic diffusion. This assumption can be tested by comparing the τ_i in Table 6 with the terminal times from linear viscoelastic mechanical data. Figure 14 shows the τ_i, plotted as log τ vs w_1, together with mechanically measured terminal times, corrected to the conditions of our experiments with the free volume theory. The solid line shows the terminal times from the rheological data of Akovali[10] on polystyrene melts. These were corrected using the shift factor suggested by Vrentas and Duda,[17] as described in part 1:

$$\tau(T,w_1,M_2) = \frac{D_2(T_0,w_{10},M_{20})}{D_2(T,w_1,M_2)}\tau(T_0,w_{10},M_{20}) \quad (17)$$

where D_2 means the polymer self-diffusion coefficient and the subscripts 0 denote the reference conditions; the free volume theory enables convenient evaluation of the ratio on the right. The dashed line in Figure 14 shows the terminal times measured by Richards and Prud'homme,[11] using their modification of the Vrentas–

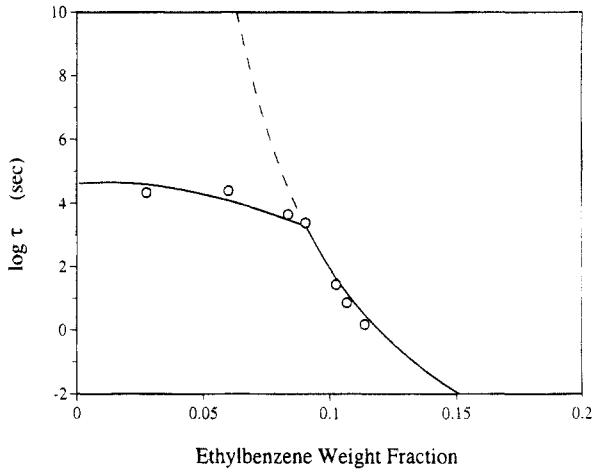

Figure 15. Plot of log τ_1 vs w_1 showing the values extracted from viscoelastic sorption data together with a fit based on the free volume theory accounting from trapped free volume below the glass transition. The fit employs the viscoelastic superposition suggested by Vrentas et al.[17] and assigning $\tau_{10} = 2 \times 10^5$ s for pure polystyrene at 100 °C.

Duda free volume theory (capable of correlating their rheological data) to correct to our experimental conditions.

Figure 14 suggests that τ_2, determined from the protracted relaxation to equilibrium in the pseudosigmoid weight-uptake curves (see Table 1 and Figures 7–9), is the terminal relaxation time. We emphasize, however, that this assignment is tentative since the data for τ_2 are limited (only three values). Note also that the τ_2 are closer to the terminal times from Akovali's data than those from Richard's even though the latter were measured at conditions closer to our sorption experiments than the former; this discrepancy underscores the tentative nature of the assignment of τ_2. Clearly, additional measurements, varying the polymer molecular weight, are needed in order to confirm that τ_2 is indeed the terminal time.

The relaxation times τ_1, determined from fitting the short-time portion of the two-stage and pseudosigmoid weight-uptake curves, are clearly not the terminal time, since they are significantly smaller, by at least 3 orders of magnitude, than either estimate of the terminal times at the sorption conditions, as shown in Figure 14. Interestingly, the τ_1 appear to level to a nearly constant value of $\simeq 2 \times 10^4$ s for w_1 below about 0.09, reminiscent of the behavior found for D_{12} (see Figure 11).

In order to associate τ_1 with a mechanical relaxation time and to explain the dependence of the τ_1 on w_1, we proceeded as follows. First, a reference relaxation time for pure polystyrene was found which, when corrected to our sorption condition via the liquid-state free volume theory (i.e., using eqs 14 and 17), gave good agreement with our data for $w_1 > 0.09$. This gave a reference time of $\simeq 2 \times 10^5$ s for pure PS melt at 100 °C. We then used the free volume theory modified for the glassy state (i.e., eq 14 with eq 16 added) for $w_1 < 0.09$. Figure 15 shows the data and the free volume calculation, plotted as log τ vs w_1. The agreement between the data and calculation is excellent considering that only one adjustable parameter (the reference relaxation time, τ_{10}) appears in the free volume theory.

Mechanical relaxation times characteristic of the transition region have been measured in shear creep experiments for pure polystyrene in the neighborhood of 100 °C. τ_{10} is considerably larger than the effective relaxation time characterizing the onset of the α relax-

ation (i.e., the transition zone) reported by Plazek et al.[8] (≃10^2 s at 95 °C). Instead, τ_{10} seems to correspond to relaxation times near the end of the transition zone since it shows good agreement with the peak time in the retardation spectrum associated with the α relaxation in polystyrene; Riande et al.[9] reported 3 × 10^5 s at 100 °C for this quantity. The comparison suggests that the second stage of the two-stage uptake process observed just below the glass transition is controlled by local segmental reorganizations typical of those associated with the long time-scale end of the α mechanical dispersion. This is consistent with Durning's[40] analysis which indicated that a relaxation time near the end of the transition zone controlled two-stage uptake in the system poly(methyl methacrylate)/methyl acetate.

The foregoing analysis of relaxation times is broadly consistent with Vrentas et al.'s study[41] of linear viscoelastic diffusion in poly(vinyl acetate)–fluid systems via oscillatory sorption. (In oscillatory sorption one varies the fluid activity in the reservoir sinusoidally (i.e., $\delta a(t) = a_0 \sin \omega t$ in eq 8) and determines the steady-periodic fluid uptake.) By oscillating the activity of the fluid in the reservoir over a range of frequencies, they found three regions of Fickian diffusion separated by two zones of viscoelastic diffusion, each controlled by a distinct relaxation process. The dominant relaxation times associated with each viscoelastic zone seemed to correspond to times in the transition and terminal zones.

***D'/D* and the Moduli.** Table 3 lists values of k_0 and g_1 determined from the analysis of the sorption data. Both of these depend on the moduli G_i in the generalized Maxwell model (see eqs 40–42 and eqs 5 and 49). The data analysis shows that both k_0 and g_1 are nearly constant with composition over the range studied with values $k_0 \simeq 30$ and $g_1 \simeq 0.994$.

Recall that $k_0 = D'/D$ is the ratio of the high-frequency mechanical modulus (either shear or longitudinal, depending on the model considered) to the bulk osmotic modulus (eq 5). If the solution thermostatics is represented by the Flory–Huggins theory, f in eq 5 can be expressed

$$f = \ln \varrho_1\hat{V}_1 + \varrho_2\hat{V}_2 + \chi\varrho_2\hat{V}_2 \qquad (18)$$

Differentiation gives

$$-\frac{\partial f}{\partial \ln w_2} = \varrho\hat{V}_1\varrho_2\hat{V}_2[(\varrho_1\hat{V}_1)^{-1} - 1 - 2\chi] \qquad (19)$$

A natural choice for the high-frequency modulus, G_0, is the value for pure, glassy polystyrene ($G_0 \simeq 2 \times 10^{10}$ dyn/cm^2 [42]). Figure 16 shows the k_0 calculated using eqs 5, 19, and 49 with the assumed constant value of G_0 plotted against w_1 for two values of χ; the density data needed for this calculation were taken from refs 43 and 44. The calculation predicts that k_0 increases monotonically with w_1, in contrast with the data which show practically no dependence on composition. Nonetheless the value of $k_0 \simeq 30$ extracted from the sorption data is reasonable in order of magnitude; it coincides with the prediction for $\chi = 0.05$ at $w_1 \simeq 0.15$. It is unclear whether the disagreement in trend with w_1 arises from a weakness in the theory for linear viscoelastic diffusion or the approximations made in predicting k_0 from first principles (e.g., constant G_0). Sorption experiments involving other solvents and high-frequency dynamic mechanical data on concentrated polymer solutions could clarify this point.

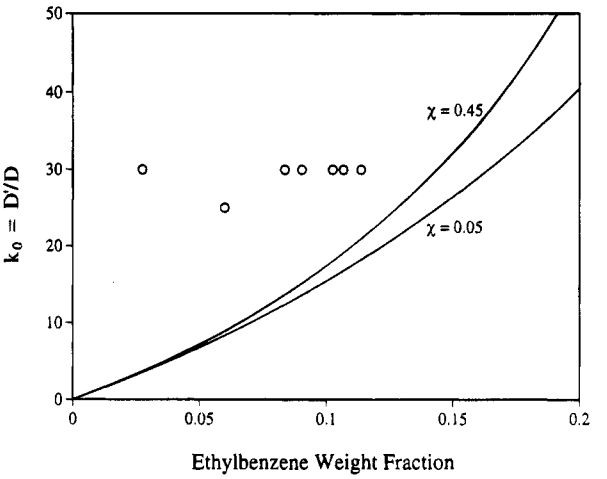

Figure 16. Plot of k_0 vs w_1 showing the prediction using the Flory–Huggins solution theory and the assumption that G_0 = constant = 2 × 10^{10} dyn/cm^2 (the glassy state value for pure polystyrene); values of χ in the Flory–Huggins expression are indicated.

Before discussing g_1, we point out an interesting observation regarding the composition dependence of k_0 predicted in Figure 16. The theory for viscoelastic diffusion employing the Maxwell model for the relaxation function predicts that the parameter k_0 controls the amount of fluid absorbed in the initial stage of two-stage sorption; i.e., it controls the height of the "knee" appearing initially in the two-stage uptake curves. In particular, the knee height varies inversely with k_0. Consequently, the dependence of k_0 on w_1 predicted in Figure 16 corresponds to a sequence of two-stage uptakes in which the knee height relative to the equilibrium uptake decays with increasing w_1. This sequence is not seen in our experiments, nor was it observed by Odani et al.[33,45–47] for amorphous polymer–fluid systems (as mentioned above, we are not entirely clear why this discrepancy exists). Interestingly, however, exactly this sequence was observed for semicrystalline polymer–fluid systems by Odani and others.[46,48] While we cannot reconcile why these differences appear for the semicrystalline polymers at present, it is clear that the theory offers the possibility of explaining such differences in terms of mechanical and/or thermostatic properties.

For the sigmoidal sorption curves featuring a protracted approach to equilibrium, two Maxwell elements in parallel were used in the modeling. Within the accuracy of the data the analyses show that $g_1 = G_1/G_0$ is constant at 0.994. By eqs 41 and 42, $g_2 = G_2/G_0$ is also constant at 0.006. We emphasize that these are rough estimates since the second relaxation is difficult to discern, i.e., since these parameters were determined solely from the slow approach of the fluid uptake to the final value. It seems natural to connect the larger modulus, G_1, associated with the shorter relaxation time τ_1, with the glassy modulus and to connect the smaller modulus G_2, associated with the longer relaxation time τ_2, with the plateau modulus. The ratio of the glassy to the plateau modulus for pure polystyrene is about 4000;[42] the ratio G_1/G_2 determined from our data is about 170, more than an order of magnitude less. Nonetheless, the large value of this ratio suggests again that the secondary relaxation in the sigmoidal weight-uptake curves is the terminal process.

Summary and Conclusion

A quantitative analysis of the Fickian weight-uptake curves observed at the highest ethylbenzene contents via the classical theory gave diffusion coefficients $D \sim O(10^{-10}$ cm^2/s); these increase with ethylbenzene content. The values and trend are consistent with diffusion coefficients measured by Duda et al.[34] at much higher temperatures, when extrapolated to our conditions using the free volume theory.

We modeled the non-Fickian sorption data using the common one-dimensional diffusion equation derived from two distinct nonequilibrium thermodynamic treatments of diffusion in a mixture of a viscoelastic material and a simple fluid.[2,3] The generalized Maxwell model was used for the relaxation function of the mixture; a set of dimensionless parameters ($k_0 = D'/D$, $g_i = G_i/G$, $k_i = D\tau_i/l^2$) controls the predictions. We fit the non-Fickian data by trial and error manipulation of the dimensionless parameters and made subsequent comparisons of the dimensional transport properties with independently measured reference data.

For the two-stage weight-uptake curves, the data were modeled best using a single Maxwell element. In all cases, the predictions captured the initial stage of two-stage uptake curves perfectly. However, for runs where the ethylbenzene weight fraction interval, δw_1, significantly exceeded ~0.01, the data during the second, relaxation-controlled stage approached equilibrium more rapidly than the theory predicted; the addition of more Maxwell elements to the model could not improve the long time prediction. This discrepancy is a manifestation of weak nonlinearities in the sorption experiments: If the mean ethylbenzene fraction increases too much in the second stage, the relaxation time controlling the fluid uptake decreases, causing a more rapid fluid uptake than predicted in the linearized theory.

For the pseudosigmoid weight-uptake curves, with a slow drift to the final equilibrium, two Maxwell elements in parallel gave the best representation of the data; the second element with a long relaxation time nicely captured the slow approach to the final equilibrium uptake.

The modeling enabled calculation of physical properties D_{12}, τ_1, τ_2, k_0, and g_1 from the non-Fickian sorption data. The diffusion coefficient D_{12} remained nearly constant with composition below $w_1 = 0.09$, at $\sim 10^{-12}$ cm^2/s, while at higher ethylbenzene contents, it increased monotonically with w_1. The data were compared with extrapolations to our conditions via free volume theory of the D_{12} measured by the Penn State group at much higher temperatures[34] and with values deduced from self-diffusion data measured near our experimental conditions.[35] Assuming that the polymer solution has an equilibrium liquid structure above T_g ($w_1 > 0.09$) but has excess or trapped free volume below T_g gave very good agreement between the data and the free volume extrapolations. We emphasize that the parameters in the free volume theory were completely determined from independent measurements reported in the literature.

The relaxation times τ_1 and τ_2 were compared with mechanically measured values characterizing the transition and terminal zones of the linear viscoelastic spectrum in pure polystyrene. The comparison was made using the free volume theory to correct for the conditions of our experiments. The large relaxation time, τ_2, showed rough agreement with the terminal time, although the correspondence was not definitive. The shorter time, τ_1, corresponded well with the longer mechanical relaxation times in the transition zone. The trend in τ_1 with w_1 was reminiscent of that in D_{12}: Below $w_1 \simeq 0.09$, where the mixture is glassy, τ_1 remained practically fixed at a value of $\sim O(10^4$s), while at higher values of $w_1 \simeq 0.09$, where the mixture is liquidlike, τ_1 decreases monotonically with w_1. As in the case of the diffusion coefficients, the free volume theory modified to account for trapped free volume below the glass transition gave an excellent correlation of the trend in τ_1 with composition.

The parameter k_0 gives the ratio of the high-frequency mechanical modulus of the dry polymer (the shear modulus according to DT[2] but the longitudinal modulus according to Lustig[3]) to the bulk osmotic modulus of the mixture. We found values of k_0 around 30 over the entire concentration range examined ($0 < w_1 < 0.15$), whereas a simple calculation based on the Flory–Huggins solution theory predicts that it should increase monotonically with w_1 from zero in the concentrated polymer regime. Although the value of 30 is reasonable in order of magnitude for mixtures having about 10–15 wt % ethylbenzene, the exact reasons for the discrepancy in trend with w_1 remain unclear.

The linearized theory for viscoelastic diffusion is clearly capable of modeling the non-Fickian differential sorption data reported in part 1 and in previous studies. The success in accounting for the magnitudes and composition dependencies of the transport properties calculated by curve fitting the data in terms of independently measured values is the strong evidence supporting the validity of the theory.

Acknowledgment. This work was supported by the National Science Foundation (Grant CTS-89-19665) and by the DuPont and Goodrich companies.

Appendix A

The constitutive development by DT rests on a minimal set of balance laws describing the mixture thermodynamics; these are the species continuity equations, balances of linear and angular momentum for the mixture, and an energy balance for the mixture. This set implies the barycentric velocity, $\mathbf{v}$, and the temperature, T, defining the average motion and thermal history of the mixture, can be assigned arbitrarily and independently if the liquid mass flux (relative to $\mathbf{v}$), $\mathbf{j}_1$, the stress in the mixture, $\mathbf{\Pi}$, the specific internal energy, $\hat{U}$, and the heat flux, $\mathbf{q}$, are assumed to depend on the current component mass densities, ϱ_1 and ϱ_2, and on the history of $\mathbf{v}$ and T, and, possibly, their gradients. This justifies applying Coleman's[25] procedure for deducing the thermodynamic "admissibility conditions", i.e., the restrictions on the constitutive functionals imposed by the entropy inequality.

Reference 2 uses the entropy inequality in the form

$$\varrho \frac{D\hat{S}}{Dt} + \nabla \cdot \mathbf{s} - \varrho \frac{Q}{T} \equiv \sigma \geq 0 \tag{20}$$

where $\varrho = \varrho_1 + \varrho_2$ is the total mass density of the mixture, $\hat{S}$ is the specific entropy of the mixture, and $\mathbf{s}$ is the entropy flux, assumed to obey

$$\mathbf{s} = \mathbf{q}/T - \frac{\varrho}{T}\left[\frac{\partial \hat{A}}{\partial \varrho_1}\mathbf{j}_1 - \frac{\partial \hat{A}}{\partial \varrho_2}\mathbf{j}_2\right] \tag{21}$$

where $\hat{A} \equiv \hat{U} - T\hat{S}$ is the specific free energy. Equation

21 mimics the well-established result for mixtures of simple fluids. The free energy functional was assumed to be in the form

$$\hat{A} = \hat{A}(\varrho_1,\varrho_2;T(s),\mathbf{F}(s)) \tag{22}$$

where $g(s)$ means the history of g; $\mathbf{F}$ means the polymer's deformation gradient.

Combining the energy balance with eqs 20–22 and assuming the smoothness properties for the functional $\hat{A}(\varrho_1,\varrho_2;T(s),\mathbf{F}(s))$ discussed by Coleman,[25] DT[2] proved the admissibility condition

$$\mathbf{j}_1\cdot\nabla\varrho\left[\frac{\partial\hat{A}}{\partial\varrho_1} - \frac{\partial\hat{A}}{\partial\varrho_2}\right] \le 0$$

on $\mathbf{j}_1$, for an isothermal process. A sufficient condition satisfying the above was adopted

$$\mathbf{j}_1 = -\Omega\nabla\varrho\left[\frac{\partial\hat{A}}{\partial\varrho_1} - \frac{\partial\hat{A}}{\partial\varrho_2}\right] \tag{23}$$

where Ω is a positive scalar.

Equation 23 was put in a form consistent with the widely used result from linear irreversible thermodynamics (see ref 26, for example)

$$\mathbf{j}_1{}^2 \equiv \varrho_1(\mathbf{v}_1 - \mathbf{v}_2) = -\frac{\Omega}{w_2{}^2}\nabla\mu_1 \tag{24}$$

where the local fluid chemical potential per unit mass, μ_1, has the definition

$$\mu_1 = \frac{\partial}{\partial\varrho_1}\varrho\hat{A} + \text{const} = (\varrho_2\hat{V}_2)^2\frac{\partial}{\partial\varrho_1}(\Phi/\varrho_2\hat{V}_2) + \text{constant} \tag{25}$$

Here, Φ means the free enthalpy density. In the special case of infinitesimal displacement gradients at constant temperature and pressure, a Gibbs–Duhem relation was shown to hold

$$\nabla\frac{\partial}{\partial\varrho_2}\varrho\hat{A} \simeq -\frac{w_1}{w_2}\nabla\frac{\partial}{\partial\varrho_1}\varrho\hat{A};\quad ||\mathbf{F}-\boldsymbol{\delta}|| \ll 1,\ \text{fixed } T \text{ and } P \tag{26}$$

(The reader should note that this relation was incorrectly stated in eq IV.3 of ref 2.) Combining eqs 23 and 26 gives 24 with μ_1 defined by eq 25 but containing the nonequilibrium free energy functional, eq 22.

Results relevant to concentrated solutions of linear, entangled polymers were developed by considering appropriate functional forms for Φ. The form

$$\Phi = \Phi^{\mathrm{m}} + \Phi^{\mathrm{f}} \tag{27}$$

was assumed, where Φ^{m} is the quilibrium mixing free energy and Φ^{f} is a nonequilibrium, relaxing contribution from the polymer, depending on its deformation history. Specific results for Φ^{f} were derived from the transient network and reptation models assuming infinitesimal deformation of the polymer. A common, single memory-integral form was found from these two models, weighting the history of the polymer dilatation rate with the same relaxation function that appears in kinetic theory treatments of the extra stress based on these models. (The reader should note that the treatment also yields an admissibility condition relating the pressure tensor, $\mathbf{\Pi}$, to the free energy density, which yields the same expressions for the extra stress as from the standard kinetic theory.)

For a 1D process, the concentration history prescribes the polymer deformation history so Φ^{f} and the corresponding part of μ_1 could be expressed as functionals of the concentration history in this case. Assuming 1D isothermal, isobaric transport, the result for μ_1 is

$$\mu_1 = \frac{RT}{M_1}f + \frac{V_1G_0}{M_1}\varrho_2\hat{V}_2\hat{V}_1\int^t\varphi(t-t',C')\frac{\partial C'}{\partial t'}\,dt' + \text{constant};\quad ||\mathbf{F}-\boldsymbol{\delta}|| \ll 1,\ \text{fixed } T \text{ and } P,\ 1\text{D} \tag{28}$$

where C' means $C(X,t')$, M_1 is the fluid's molecular weight, and V_1 is its molar volume. The first term on the right, derived from Φ^{m}, gives the equilibrium chemical potential; the dimensionless function f depends only on composition. The second term, derived from Φ^{f}, gives the effect of diffusion-induced deformation of polymer on the chemical potential. Here φ is a normalized relaxation function, characterizing the linear viscoelastic mechanical response of the mixture in shear; $G(C)$ means the mixture's instantaneous or high-frequency (shear) modulus. Combining eqs 24 and 28 leads to an expression for the fluid flux in one dimension.

Appendix B

Lustig et al.[3,27] used the rational thermodynamic theory of mixtures[28] to derive the diffusion fluxes for a mixture of $N-1$ diffusing and reacting fluids in a viscoelastic material (fluid or solid). Here we summarize the key ideas and results for the case of a nonreactive binary mixture of a fluid and a viscoelastic liquid; we retain the original notation used by Lustig, unless otherwise noted.

The development rests on a larger set of balance laws than in DT's treatment: Species continuity equations, linear and angular momentum balances for each species, linear and angular momentum balances for the mixture, an energy balance for the mixture, and an entropy balance for the mixture. The species momentum balances (force balances on each component) include partial stresses, $\mathbf{T}_i$, which give each component's contribution to the pressure tensor, $\mathbf{\Pi}$ (the $\mathbf{T}_i$ are defined such that $\Sigma_i(\mathbf{T}_i + \mathbf{j}_i^2/\varrho_i) = -\mathbf{\Pi}$), and the interaction force exerted on each species by the others, $\mathbf{m}_i{}^+$. The balances are supplemented by constitutive relationships for $\mathbf{T}_i$, $\mathbf{m}_i{}^+$, the mixture's specific internal energy $\hat{U}$, entropy, $\hat{S}$, heat flux, $\mathbf{q}$, and entropy flux, $\mathbf{s}$ (in Lustig's notation $\mathbf{\Pi} = -\mathbf{T}$, $\hat{U} = \epsilon$, $\hat{S} = \eta$, $\hat{A} = \psi$, and $\mathbf{s} = \phi$), to give a closed field theory. Each constitutive quantity is assumed to depend on the set

$$\{\varrho_i,\ \nabla\varrho_i,\ \mathbf{v}_1 - \mathbf{v}_2,\ \nabla T,\ T(s),\ \mathbf{F}(s)\} \tag{29}$$

where $\mathbf{F}$ means the polymer deformation gradient. Including the histories, $T(s)$ and $\mathbf{F}(s)$ capture the aspect of memory. The problem of admissibility (i.e., of satisfying the entropy inequality) was solved by Liu's method of Lagrange multipliers.[28,30] Among other things, the admissibility calculation yields connections between each of the partial stress tensors and the mixture's specific free energy, $\hat{A}$, and supplies a "reduced" entropy inequality restricting the functional form of the interaction forces, $\mathbf{m}_i{}^+$.

Lustig[27] specialized the general results to the case of "simple" mixtures, where $\nabla\varrho_i$ are deleted from the list

(29). Here, the free energy must have the form

$$\varrho\hat{A} = \varrho_1\hat{A}_1(\varrho_1,T(s)) + \varrho_2\hat{A}_2(\varrho_2,T(s),\mathbf{F}(s)) \quad (30)$$

and the partial stresses are

$$\mathbf{T}_1 = -\varrho_1^2\frac{\partial\hat{A}_1}{\partial\varrho_1}\boldsymbol{\delta} \equiv -p_1\boldsymbol{\delta} \quad (31)$$

$$\mathbf{T}_2 = -\varrho_2^2\frac{\partial\hat{A}_2}{\partial\varrho_2}\boldsymbol{\delta} + 2\varrho\mathbf{F}\cdot\frac{\partial\hat{A}_2}{\partial\mathbf{C}}\cdot\mathbf{F} \equiv -p_2\boldsymbol{\delta} + 2\varrho\mathbf{F}\cdot\frac{\partial\hat{A}_2}{\partial\mathbf{C}}\cdot\mathbf{F} \quad (32)$$

where $\mathbf{C} = \mathbf{F}^+\cdot\mathbf{F}$ is the right Cauchy–Green tensor for the polymer and the p_i are "partial pressures". Note that the fluid behaves as an inviscid material in the simple mixture model and mechanical dissipation arises entirely from the polymer.

Subtracting the polymer from the fluid momentum balance gives the interaction force on the fluid, $\mathbf{m}_1^+$. Neglecting body forces and inertial terms, introducing a representation of $\mathbf{m}_1^+$ appropriate for an isotropic material, and satisfying the reduced entropy inequality lead to

$$\mathbf{j}_2^1 \equiv \varrho_1(\mathbf{v}_1 - \mathbf{v}_2) = \frac{\varrho_1\varrho_2}{\varrho m_{12}}\left(\frac{1}{\varrho_1}\nabla\cdot\mathbf{T}_1 - \frac{1}{\varrho_2}\nabla\cdot\mathbf{T}_2\right); \quad \text{isothermal, no body forces or inertia} \quad (33)$$

in an isothermal system. Here, m_{12} is a binary drag coefficient. Combining the last three equations and introducing the fluid chemical potential, $\mu_1 = \partial(\varrho_1\hat{A}_1)/\partial\varrho_1 + \text{constant} \equiv RTf/M_1 + \text{constant}$, and the binary-mutual diffusion coefficient, D_{12}, gives

$$\mathbf{j}_1^2 = -\frac{D_{12}}{\varrho_2\hat{V}_2}\nabla\varrho_1 - \frac{D_{12}M_1}{RTw_2^2}\left(\frac{\partial f}{\partial w_1}\right)^{-1}\nabla\cdot\mathbf{T}_2 \quad (34)$$

Equation 34 indicates that the fluid flux in the polymer is the sum of Fick's law and a term involving the polymer partial stress, presumably responsible for non-Fickian or viscoelastic effects.

Lustig[27] modeled the polymer as a viscoelastic solid. He assumed $\varrho_2\hat{A}_2$ is a sum of an equilibrium contribution dependent only on the current polymer deformation and giving rise to long-time dilational and multiaxial elasticity and a relaxing contribution dependent on the polymer deformation history and giving rise to viscoelasticity. For a viscoelastic liquid, the first contribution is absent. Adopting Lustig's representation of the relaxing contribution gives

$$T_{2,xx} = \frac{(\varrho_2\hat{V}_2)^{-1}}{2}\int^t M_\Delta(t-t',\varrho_2\hat{V}_2(t'))\frac{\partial(\varrho_2\hat{V}_2(t'))^{-2}}{\partial t'}\,dt' \quad (35)$$

for the only nontrivial component of $\mathbf{T}_2$ in 1D sorption. Here M_Δ means the longitudinal relaxation modulus of the polymer, given by $^4/_3G_\Delta + K_\Delta$ where G_Δ and K_Δ are the shear and dilatational relaxation moduli, respectively.

Combining eqs 34 and 35 and converting to polymer material coordinates (i.e., $x \to X$, $\varrho_i \to C$) leads to eq 4, but with the definition

$$g(C) = \frac{M(C)}{M_0(\varrho_2\hat{V}_2)^2} \quad (36)$$

with $M(C)$ being the instantaneous longitudinal modulus of the mixture and $M_0 = M(C=0)$. Also, with Lustig's derivation

$$\varphi(t-t',C') = \frac{M_\Delta(t-t',\varrho_2\hat{V}_2(C'))}{M_0\varrho_2\hat{V}_2(C')} \quad (37)$$

and

$$D' = D\frac{M_0V_1}{RT(-\partial f/\partial\ln w_2)}\frac{1}{w_2\varrho_2\hat{V}_2} \quad (38)$$

which are slightly different from the corresponding results found by DT.

Appendix C

Lustig[3,27] discusses appropriate boundary conditions for mass transport problems involving phase interfaces. The key relation is a jump linear momentum balance across the phase boundary, asserting that the total normal stress be continuous across the discontinuity. Neglecting the inertial contributions from diffusion (i.e., assuming $-\boldsymbol{\Pi} = \mathbf{T}_1 + \mathbf{T}_2$), one finds for a simple mixture

$$-p_1 + T_{2,xx} = -p \quad (39)$$

at the film surface in 1D sorption (see Figure 1). Here, p is the total pressure in the reservoir, assuming the reservoir contains pure fluid, $p_1 = \varrho_1^2\,\partial\hat{A}/\partial\varrho_1$ is the pressure in the mixture contributed by the fluid, and the second term on the left is the normal stress in the mixture contributed by the polymer, given by eq 35 of Appendix B.

Although the details differ, the mathematical structure of eq 39 is the same as the boundary condition based on continuity of the fluid chemical potential at the phase boundary (cf. eqs 6 and 39 with eq 35 after introducing specific function for $p_1(\varrho_1)$ and conversion to the composition scale C).

Appendix D

Here we derive the viscoelastic model for $\delta C(X,t)$ and summarize a nice method of calculating the relative weight uptake. We use the generalized Maxwell model as a robust representation of the relaxation function, φ, appearing in the flux expression, eq 4.

The generalized Maxwell fluid's response is governed by a set of n relaxation times, τ_i, n moduli, G_i, and n viscosities, η_i, interrelated by

$$G_i = \eta_i/\tau_i; \quad i = 1, 2, ..., n \quad (40)$$

The relaxation function and instantaneous modulus are

$$\varphi(t) = \sum_{i=1}^{n} g_i e^{-t/\tau_i} \quad (41)$$

and

$$G_0 = \sum_{i=1}^{n} G_i \quad (42)$$

respectively, where $g_i = G_i/G_0$. This leads to the linear

diffusion equation

$$\frac{\partial \delta C}{\partial t} = D\frac{\partial^2 \delta C}{\partial X^2} + D'\frac{\partial^2}{\partial X^2}\int^t \sum_{i=1}^{n} g_i e^{-(t-t')/\tau_i}\frac{\partial \delta C}{\partial t'}\,dt' \quad (43)$$

where, as a result of linearization, all of the physical properties appearing on the right are independent of δC.

Initial conditions and two boundary conditions are needed to solve eq 43. The initial conditions correspond to a film at rest for a long time with a uniform fluid concentration equal to C^-:

$$\left.\begin{aligned}\delta C &= 0\\ \frac{\partial \delta C}{\partial t} &= 0\end{aligned}\right\} \quad \text{for } t = 0 \text{ and } 0 \le X \le l \quad (44)$$

The first boundary condition reflects that the flux vanishes at the film/substrate interface ($X = 0$) or, equivalently, at the film center line for a laterally-constrained, free-hanging film (see Figure 1):

$$0 = D\frac{\partial \delta C}{\partial X} + D'\frac{\partial}{\partial X}\int^t \sum_{i=1}^{n} g_i e^{-(t-t')/\tau_i}\frac{\partial \delta C}{\partial t'}\,dt' \quad \text{for } 0 < t < \infty \text{ and } X = 0 \quad (45)$$

The second boundary condition derives from the assumption that any disturbance of the reservoir potential communicates immediately to the mixture/reservoir interface at $X = l$ (see eq 9). For differential sorption one has $\delta a(t) = H(t)(a^+ - a^-)$ where $H(t)$ means the unit step function and, if f can be expressed as a logarithmic function of C (use of the logarithmic form for f amounts to approximating the equilibrium isotherm by Henry's law, which is reasonable for a limited range of compositions in the concentrated polymer regime), $f = \ln C/K$, K = constant, we find a particularly simple form for the second boundary condition:

$$H(t) = \frac{\delta C}{(C^+ - C^-)} + C^- Q\int^t \sum_{i=1}^{n} g_i e^{-(t-t')/\tau_i}\frac{\partial \delta C}{\partial t'}\,dt' \quad \text{for } 0 < t < \infty \text{ and } X = l \quad (46)$$

where $C^{+/-}$ means the initial/final values of concentration.

Introducing the dimensionless variables

$$u = \frac{\delta C}{C^+ - C^-};\quad s = \frac{Dt}{l^2};\quad z = \frac{x}{l} \quad (47)$$

leads to

$$u_s = u_{xx} + k_0\left(\int^s \sum_{i=1}^{n} g_i e^{-(s-s')/k_i} u_{s'}\,ds'\right)_{xx} \quad (48)$$

with

$$k_0 = D'/D;\quad k_i = D\tau_i/l^2 \quad (49)$$

governing the dimensionless concentration, u. Recall the parameter k_0 is the ratio of the high-frequency shear modulus to the osmotic bulk modulus (see eq 5); the k_i are diffusion Deborah numbers. The initial conditions become

$$\left.\begin{aligned}u &= 0\\ u_s &= 0\end{aligned}\right\} \quad \text{for } s = 0 \text{ and } 0 \le z \le 1 \quad (50)$$

while the boundary conditions are recast as

$$u_z|_{z=0} + k_0\left(\int^s \sum_{i=1}^{n} g_i e^{-(s-s')/k_i} u_{s'}\,ds'\right)_z\Big|_{z=0} = 0 \quad (51)$$

and

$$u|_{z=1} + k_0\int^s \sum_{i=1}^{n} g_i e^{-(s-s')/k_i} u_{s'}\,ds'\Big|_{z=1} = H(s) \quad (52)$$

Laplace transformation of eq 48 gives

$$\frac{d^2\bar{u}}{dz^2} - \beta(p)\bar{u} = 0 \quad (53)$$

where p is the Laplace variable and $\beta(p)$ is

$$\beta(p) = p\left[1 + k_0 p\sum_{i=1}^{n}\left(\frac{k_i g_i}{1 + k_i p}\right)\right]^{-1} \quad (54)$$

Equations 53 and 54 incorporate the initial conditions, eq 50. The boundary conditions, eqs 51 and 52, transform to

$$d\bar{u}/dz|_{z=0} = 0 \quad (55)$$

and

$$\bar{u}|_{z=1} - [p(1 + k_0)]^{-1}[1 + k_0\beta(p)/p] = 0 \quad (56)$$

The solution to eqs 53 and 54 for the transformed, scaled concentration profile is

$$\bar{u}(z,p) = [p(1 + k_0)]^{-1}[1 + k_0\beta(p)/p]\frac{\cosh(2z(\beta(p))^{1/2})}{\cosh(2(\beta(p))^{1/2})} \quad (57)$$

To analyze sorption data, a FORTRAN program was written to invert $\bar{u}(z,p)$, by performing the line integration

$$u(z,s) = \lim_{Y\to\infty}\frac{1}{2\pi i}\int_{A-iY}^{A+iY}\bar{u}(z,p)\,e^{sp}\,dp$$

numerically using the method of Crump,[31] and subsequently integrating $u(z,s)$ by Simpson's rule to find the measurable relative weight uptake, $\omega(s)$,

$$\omega(s) = M_t/M_\infty = \int_0^1 u(z,s)\,dz \quad (58)$$

References and Notes

(1) Billovits, G.; Durning, C. *Macromolecules* **1993**, *26*, 6927.
(2) Durning, C. J.; Tabor, M. *Macromolecules* **1986**, *19*, 2220.
(3) Lustig, S. R.; Caruthers, J. M.; Peppas, N. *Chem. Eng. Sci.* **1992**, *47*, 3037.
(4) Vrentas, J. S.; Duda, J. L. *J. Polym. Sci., Polym. Phys. Ed.* **1977**, *15*, 403.
(5) Vrentas, J. S.; Duda, J. L. *J. Polym. Sci., Polym. Phys. Ed.* **1977**, *15*, 417.
(6) Vrentas, J. S.; Duda, J. L.; Ling, H. C. *Macromolecules* **1988**, *21*, 1470.

(7) Vrentas, J. S.; Duda, J. L.; Ling, H. C. *J. Polym. Sci., Polym. Phys. Ed.* **1988**, *26*, 1059.
(8) Plazek, D. J.; Ngai, K. L.; Rendell, R. W. *Polym. Eng. Sci.* **1984**, *24*, 1111.
(9) Riande, E.; Markovitz, H.; Plazek, D. J.; Raghupathi, N. *J. Polym. Sci., Polym. Symp.* **1975**, *50*, 405.
(10) Akovali, G. *J. Polym. Sci., Polym. Phys. Ed.* **1967**, *5*, 875.
(11) Richards, W. D.; Prud'homme, R. K. *J. Appl. Polym. Sci.* **1986**, *31*, 763.
(12) (a) Neogi, P. *AIChE J.* **1983**, *29*, 829. (b) Durning, C. J.; Tabor, M. *Macromolecules* **1986**, *19*, 2220. (c) Cohen, Y.; Metzner, A. B. *Chem. Eng. Commun.* **1986**, *41*, 73. (d) Carbonell, R. G.; Sarti, G. C. *Ind. Eng. Chem. Res.* **1990**, *29*, 1194. (e) Jou, D.; Camacho, J.; Grmela, M. *Macromolecules* **1991**, *24*, 3597. (f) Perez-Guerrero, A. N.; Garcia-Colin, L. S. *J. Non-Equilib. Thermodyn.* **1991**, *16*, 201. (g) Edwards, B. J.; Beris, A. N. *Ind. Eng. Chem. Res.* **1991**, *30*, 873. (h) Lustig, S. R.; Caruthers, J. M.; Peppas, N. *Chem. Eng. Sci.* **1992**, *47*, 3037. (i) Morman, K. N. In *Mathematics in Industrial Problems*; Friedman, A., Ed.; Springer-Verlag: New York, 1992; Part 5. (j) Govindjee, S.; Simo, J. C. *J. Mech. Phys. Solids* **1993**, *41*, 863. (k) Goldstein, P.; Garcia-Colin, L. S. *J. Chem. Phys.* **1993**, *99*, 3913.
(13) (a) Brunn, P. O. *Physica* **1986**, *20D*, 403. (b) Bhave, A. V.; Armstrong, R. C.; Brown, R. A. *J. Chem. Phys.* **1991**, *95*, 2988.
(14) (a) Helfand, E.; Fredrickson, G. H. *Phys. Rev. Lett.* **1989**, *62*, 2468. (b) Wang, C. H. *Macromolecules* **1992**, *25*, 1524. (c) Doi, M.; Onuki, A. *J. Phys. II Fr.* **1992**, *2*, 1631.
(15) Edwards, D. A.; Cohen, D. S. *SIAM J. Appl. Math.*, submitted.
(16) Vrentas, J. S.; Jarzebski, C. M.; Duda, J. L. *AIChE J.* **1975**, *21*, 94.
(17) Vrentas, J. S.; Duda, J. L. *J. Polym. Sci., Polym. Phys. Ed.* **1977**, *15*, 441.
(18) Prager, S.; Long, F. A. *J. Am. Chem. Soc.* **1951**, *73*, 4072.
(19) Long, F. A.; Kokes, R. J. *J. Am. Chem. Soc.* **1953**, *75*, 2232.
(20) Thomas, N. L.; Windle, A. H. *Polymer* **1978**, *19*, 255.
(21) Jacques, C. H. M.; Hopfenberg, H.; Stannett, V. In *Permeability of Plastic Films and Coatings*; Hopfenberg, H. B., Ed.; Plenum: New York, 1974.
(22) Smith, M. J.; Peppas, N. A. *Polymer* **1985**, *26*, 569.
(23) Alfrey, T.; Gurnee, E. F.; Lloyd, W. G. *J. Polym. Sci., Part C* **1966**, *12*, 249.
(24) Billovits, G.; Durning, C. J. *Chem. Eng. Commun.* **1990**, *31*, 358.
(25) Coleman, B. D. *Arch. Ration. Mech. Anal.* **1964**, *17*, 1.
(26) Haase, R. *Thermodynamics of Irreversible Processes*; Addison-Wesley: Reading, Mass., 1969.
(27) Lustig, S. R. Ph.D. Dissertation, Purdue University, West Lafayette, IN, 1989.
(28) Muller, I. *Thermodynamics*; Pittman: London, 1985.
(29) Vrentas, J. S.; Duda, J. L. In *Encyclopedia of Polymer Science and Engineering*; Bikales, N., Kroschewitz, J., Eds.; John Wiley: New York, 1986.
(30) Liu, I. *Arch. Rat. Mech. Anal.* **1972**, *46*, 131.
(31) Crump, K. S. *J. Assoc. Comput. Mach.* **1976**, *23*, 89.
(32) Crank, J.; Park, G. S. *Diffusion in Polymers*; Academic Press: London, 1968.
(33) Odani, H.; Hayashi, J.; Tamura, M. *Bull. Chem. Soc. Jpn.* **1961**, *34*, 817.
(34) Duda, J. L.; Vrentas, J. S.; Ju, S. T.; Liu, H. T. *AIChE J.* **1982**, *28*, 279.
(35) Zgadzai, O. E.; Maklakov, A. I. *Acta Polym.* **1985**, *36*, 621.
(36) Vrentas, J. S.; Chu, C. H. *J. Appl. Polym. Sci.* **1987**, *34*, 587.
(37) Ueberreiter, K. *Angew. Chem.* **1940**, *53*, 247.
(38) Hocker, H.; Blake, G. J.; Flory, P. J. *Trans. Faraday Soc.* **1971**, *67*, 2251.
(39) Fox, T. G.; Loshaek, S. *J. Polym. Sci.* **1955**, *15*, 371.
(40) Durning, C. J. *J. Polym. Sci., Polym. Phys. Ed.* **1985**, *23*, 1831.
(41) Vrentas, J. S.; Duda, J. L.; Huang, W. J. *Macromolecules* **1986**, *19*, 1718.
(42) Tobolsky, A. V.; Mark, H. F. *Polymer Science and Materials*; Wiley: New York, 1971.
(43) Barlow, A. J.; Lamb, J.; Matheson, A. J. *Proc. R. Soc. London* **1966**, *A292*, 322.
(44) Hocker, H.; Blake, G. J.; Flory, P. J. *Trans. Faraday Soc.* **1971**, *67*, 2251.
(45) Kishimoto, A.; Fujita, H.; Odani, H.; Kurata, M.; Tamura, M. *J. Phys. Chem.* **1960**, *64*, 594.
(46) Odani, H.; Kida, S.; Kurata, M.; Tamura, M. *Bull. Chem. Soc. Jpn.* **1961**, *34*, 571.
(47) Odani, H.; Kida, S.; Tamura, M. *Bull. Chem. Soc. Jpn.* **1966**, *39*, 2378.
(48) Laatikainen, M.; Lindstrom, M. *J. Membr. Sci.* **1986**, *29*, 127.